AD-A084 648 SYSTEMS SCIENCE AND SOFTWARE LA JOLLA CA F/G 18/3
SPHERICALLY SYMMETRIC NUMERICAL SIMULATION OF THE SRI GROUT SPH--ETC(U)
OCT 78 N RIMER, K LIE DNA001-77-C-0099
UNCLASSIFIED SSS-R-79-3831 DNA-4794T NL

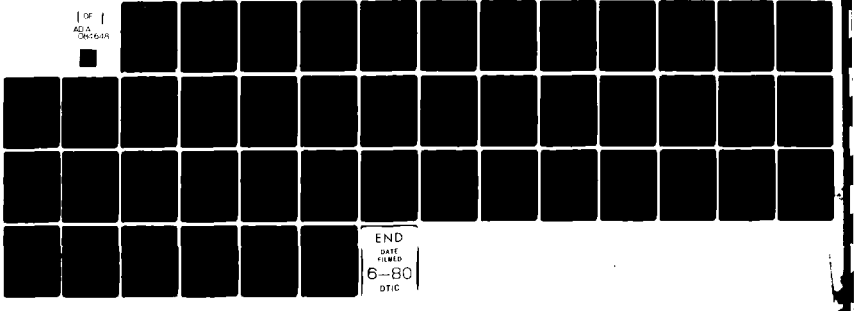

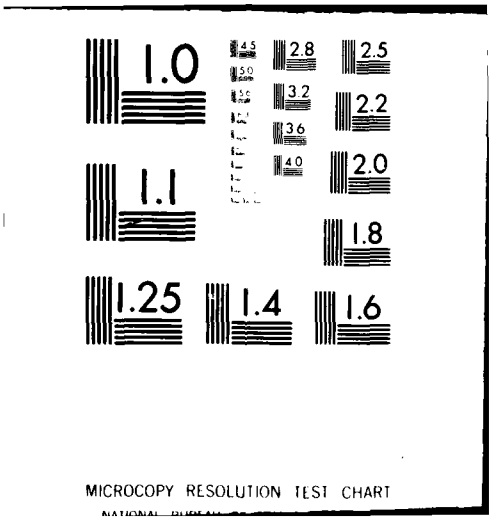
1.0
1.1
1.25
1.4
1.6
1.8
2.0
2.2
2.5
2.8
3.2
3.6
4.0
4.5
5.0
MICROCOPY RESOLUTION TEST CHART

LEVEL III

12

DNA 4794T

SPHERICALLY SYMMETRIC NUMERICAL SIMULATION OF THE SRI GROUT SPHERES CONTAINMENT EXPERIMENTS

Systems, Science and Software, Inc.
P.O. Box 1620
La Jolla, California 92038

31 October 1978

Topical Report for Period 1 January 1978—31 October 1978

CONTRACT No. DNA 001-77-C-0099

APPROVED FOR PUBLIC RELEASE;
DISTRIBUTION UNLIMITED.

THIS WORK SPONSORED BY THE DEFENSE NUCLEAR AGENCY
UNDER RDT&E RMSS CODE B345077462 J24AAXYX98349 H2590D.

Prepared for
Director
DEFENSE NUCLEAR AGENCY
Washington, D. C. 20305

Destroy this report when it is no longer needed. Do not return to sender.

PLEASE NOTIFY THE DEFENSE NUCLEAR AGENCY, ATTN: STTI, WASHINGTON, D.C. 20305, IF YOUR ADDRESS IS INCORRECT, IF YOU WISH TO BE DELETED FROM THE DISTRIBUTION LIST, OR IF THE ADDRESSEE IS NO LONGER EMPLOYED BY YOUR ORGANIZATION.

DNA PRINTING PLANT

UNCLASSIFIED

SECURITY CLASSIFICATION OF THIS PAGE *(When Data Entered)*

REPORT DOCUMENTATION PAGE	READ INSTRUCTIONS BEFORE COMPLETING FORM
1. REPORT NUMBER: DNA 4794T ✓	2. GOVT ACCESSION NO. / 3. RECIPIENT'S CATALOG NUMBER
4. TITLE *(and Subtitle)*: SPHERICALLY SYMMETRIC NUMERICAL SIMULATION OF THE SRI GROUT SPHERES CONTAINMENT EXPERIMENTS	5. TYPE OF REPORT & PERIOD COVERED: Topical Report for Period 1 Jan 78—31 Oct 78
	6. PERFORMING ORG. REPORT NUMBER: SSS-R-79-3831 ✓
7. AUTHOR(s): N. Rimer, K. Lie	8. CONTRACT OR GRANT NUMBER(s): DNA 001-77-C-0099 ✓
9. PERFORMING ORGANIZATION NAME AND ADDRESS: Systems, Science and Software, Inc. ✓ P.O. Box 1620 La Jolla, California 92038	10. PROGRAM ELEMENT, PROJECT, TASK AREA & WORK UNIT NUMBERS: Subtask J24AAXYX983-49
11. CONTROLLING OFFICE NAME AND ADDRESS: Director Defense Nuclear Agency Washington, D.C. 20305	12. REPORT DATE: 31 October 1978
	13. NUMBER OF PAGES: 46
14. MONITORING AGENCY NAME & ADDRESS *(if different from Controlling Office)*	15. SECURITY CLASS *(of this report)*: UNCLASSIFIED
	15a. DECLASSIFICATION/DOWNGRADING SCHEDULE

16. DISTRIBUTION STATEMENT *(of this Report)*

Approved for public release; distribution unlimited.

17. DISTRIBUTION STATEMENT *(of the abstract entered in Block 20, if different from Report)*

18. SUPPLEMENTARY NOTES

This work sponsored by the Defense Nuclear Agency under RDT&E RMSS Code B345077462 J24AAXYX98349 H2590D.

19. KEY WORDS *(Continue on reverse side if necessary and identify by block number)*

Grout Spheres
Residual Stress Fields
Hydrofracture
Fracture Initiation Pressure
Cavity Pressure

20. ABSTRACT *(Continue on reverse side if necessary and identify by block number)*

As part of the DNA stemming and containment program for underground nuclear testing, Stanford Research Institute is conducting laboratory investigations to develop a containment experiment for studying residual stress fields around an explosively generated cavity in a grout sphere. Here we present the S^3 numerical simulations of the spherically symmetric aspects of these laboratory investigations. Calculations are presented which simulate the high explosive detonation and the subsequent dynamic processes which result

DD FORM 1 JAN 73 1473 EDITION OF 1 NOV 65 IS OBSOLETE

UNCLASSIFIED

SECURITY CLASSIFICATION OF THIS PAGE *(When Data Entered)*

20. ABSTRACT (Continued)

in the formation of the compressive residual stress fields around the cavity. Results are presented showing our ability to simulate the detonation of the explosive charges in water and in grout. Preliminary results are shown for a calculational model which simulates the spherically symmetric venting and subsequent hydrofracture of the cavity.

TABLE OF CONTENTS

LIST OF ILLUSTRATIONS

LIST OF TABLES

1. INTRODUCTION

As part of the DNA stemming and containment program for underground nuclear testing, Stanford Research Institute (SRI) is conducting laboratory investigations to develop a containment experiment for studying residual stress fields around exploded cavities. Systems, Science and Software (S^3) has been asked to numerically simulate these experiments in order to increase understanding of the laboratory results and to validate our capability to calculate containment related phenomena. This report summarizes one part of our calculational effort; the simulation of the high explosive detonation and the subsequent nonlinear dynamic processes which result in the formation of a compressive residual stress field in the grout sphere surrounding the exploded cavity.

The experiment is shown schematically in Figure 1 and the experimental apparatus in Figure 2 (Figures 1 and 2 have been abstracted from an SRI report[1]). Step A of the experiment involves casting a 12 inch diameter sphere of rock matching grout (RMG) around a smaller sphere of high explosive (PETN). The explosive and detonator are sealed off from the grout by a thin layer of lucite. A tube containing the detonator wires is cast into the grout extending almost to the anticipated radius of the exploded PETN. In Step B, the grout sphere is placed in the tank shown in Figure 2, and a constant external (overburden) pressure is applied. The water in the tank is prevented from entering the grout by an impermeable coating on its surface. In Step C, the high explosive is detonated and the residual cavity gases are vented through the tube. The overburden pressure is maintained during the drillback to the cavity. In Step D, fluid is pumped into the cavity at a constant flow rate until hydrofracture. The major laboratory data consists of graphs of hydrofracture pressure vs. volume of fluid pumped into the cavity.

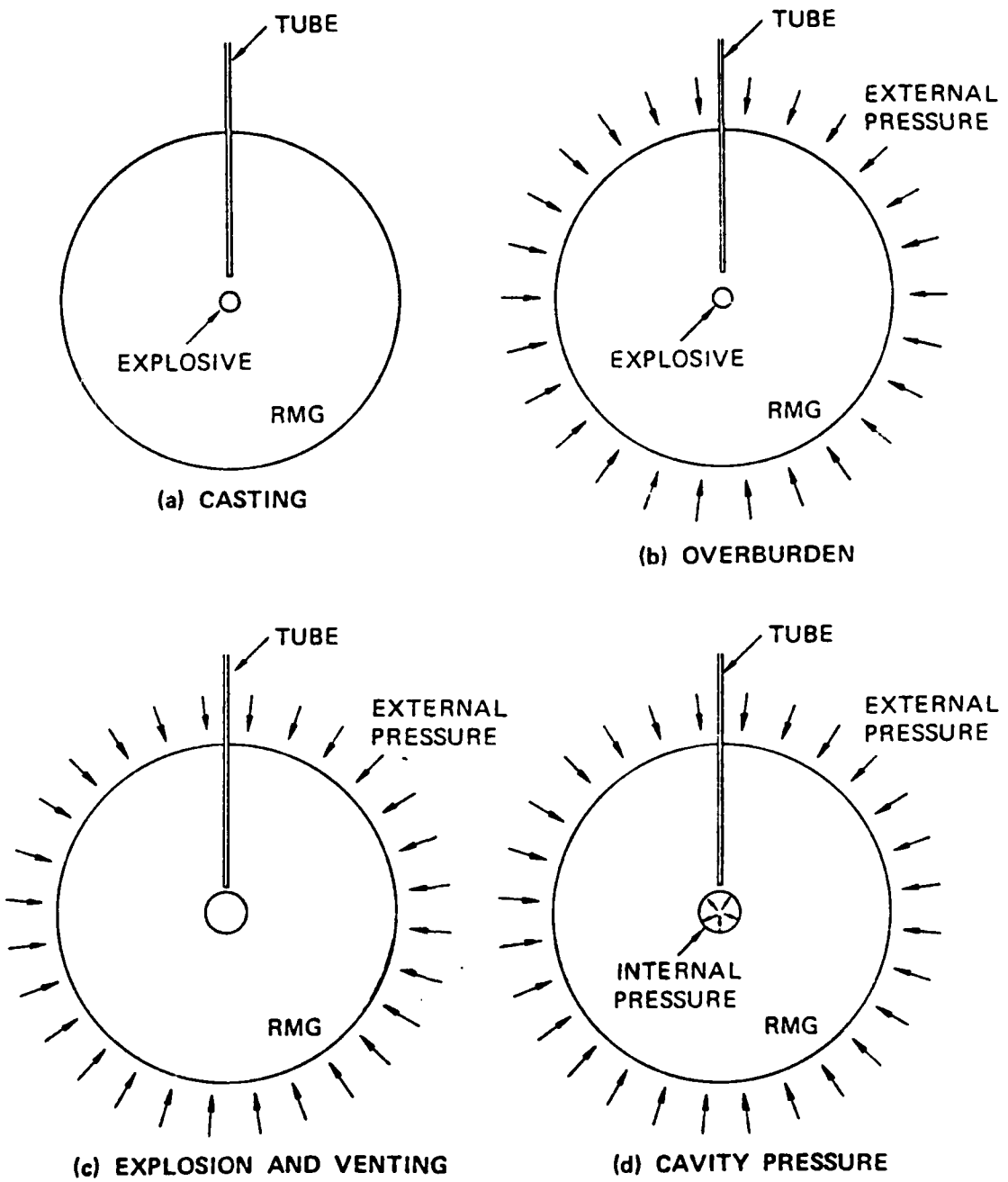

Figure 1. Sequence of operations in containment experiment.

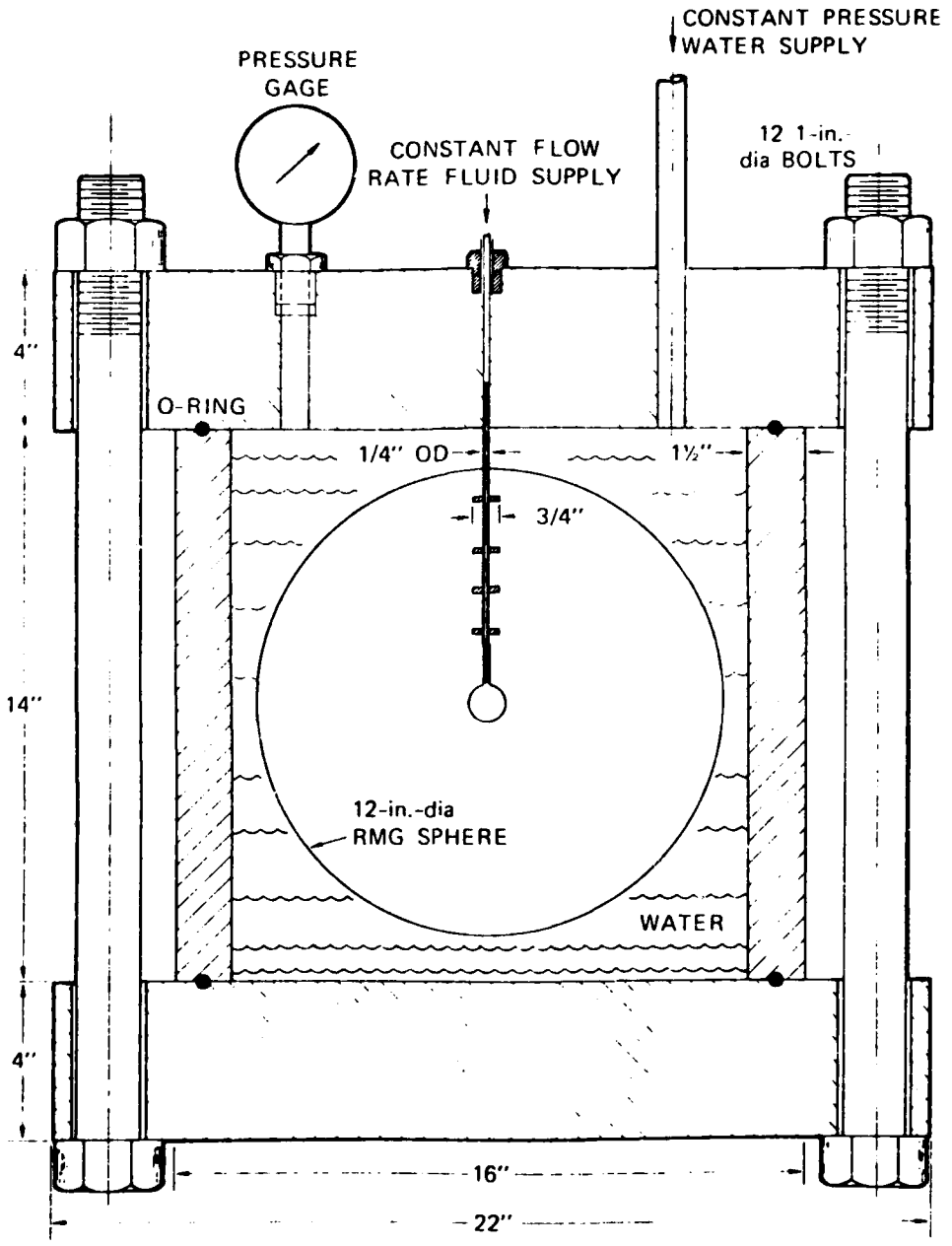

Figure 2. Containment experiment apparatus.

Hydrofracture records for exploded cavity tests are compared with records for unexploded cavities, i.e., for grout spheres with a cast-in cavity and access tube. The earliest tests showed a higher pressure was needed to initiate fracture for an exploded sphere than for an unexploded sphere and that the shapes of the records after fracture initiation were quite different. For the unexploded case, the cracks appeared to propagate at lower pressure after fracture initiation while for the exploded spheres, higher pressures were recorded after fracture initiation. These test results appeared to confirm the existence of a compressive residual stress field around the exploded cavity. However, one disturbing note was that while the exploded sphere usually fractured in a plane not including the tube, the unexploded sphere usually broke in a plane including this tube. In addition, the test results were not very reproducible.

In the last two years major improvements and modifications have been made in the test designs including varying the amount of explosive from 1/2 gm to 1/4 gm to the present 3/8 gm, improving the charge detonation, reducing the lucite shell to the present 11.4 mil thickness, changing the grout mixture to the present SRI RMG 2C4, improving the hydrofracture fluid measuring system to reduce air bubbles, and eliminating small inhomogeneities in the unexploded cavity due to a wire mesh used in its casting. However, the basic problem of reproducibility of the exploded sphere results remains. In addition the latest tests show very little difference in the fracture initiation pressures for exploded and unexploded spheres, which appears to cast some doubt on the confirmation of the residual stress field, the primary objective of the experimental study. However, recent tests in which the cavity pressure was not vented before hydrofracture result in higher fracture initiation pressures. This strongly indicates the validity of the residual stress field concept. SRI has embarked on a program of

sensor development in order to provide additional data which may be compared to analytical and numerical models of the experiment. These sensors include a strain gauge, a residual stress gauge, a surface fracture gauge, a stress gauge in the wall of the tank, and a means of measuring cavity pressure before venting.

Here we present the results of our one-dimensional spherically symmetric dynamic calculations of the detonation of the PETN explosive and the formation of the compressive residual stress field in the grout around the exploded cavity. Results are presented only for the latest test configuration, a 3/8 gm charge of PETN contained in a thin lucite shell, surrounded by a sphere of 2C4 grout. In Section 2, we describe the constitutive models and material properties used to describe the PETN explosive, the lucite shell, the 2C4 grout, and the surrounding water. In Section 3, we discuss our calculations which simulate a series of charge calibration experiments[3] in which lucite spheres containing 3/8 gm charges of PETN were detonated in the tank filled with water. Data for these tests were obtained from ytterbium pressure gauges in the water surrounding the lucite spheres and from a quartz gauge mounted in the tank wall directly below the explosive. This data is compared with our calculations and with other data for detonations in water.

In Section 4, we present our calculations of the residual stress field in the grout and compare our results with quartz gauge measurements of pressure and impulse in the wall of the tank. In Section 5 we discuss a simple calculational model of the venting and hydrofracture of the exploded cavity which allows for plastic yielding. This model assumes a spherically symmetric hydrofracture and is an extension of the analytical work of K. Narasimhan[4] for linear elastic grout behavior. (Two-dimensional axisymmetric hydrofracture calculations for the unexploded sphere case have been discussed

by Klein.[5] Similar calculations are now underway for the exploded sphere experiment.) Section 6 concludes with a summary of our results.

2. CONSTITUTIVE MODELS

In this section we discuss the constitutive models and material properties used to simulate the behavior of the PETN explosive, the lucite, and 2C4 grout, and the water in the tank.

2.1 PETN

The JWL equation of state developed at Lawrence Livermore Laboratory[6] was used to describe the behavior of the PETN explosive. The pressure P (Mb) is given as a function of internal energy E (Mb cc/cc) and V, the ratio of volume to initial volume by

$$P = A\left(1 - \frac{w}{R_1 V}\right) e^{-R_1 V} + B\left(1 - \frac{w}{R_2 V}\right) e^{-R_2 V} + \frac{wE}{V}$$

where A, B, R_1, R_2 and w are coefficients of the fit.

For the given PETN density (ρ_o = 1.0 gm/cc), Finger[7] has estimated both the Chapman-Jouget state and the coefficients for the JWL equation of state. The JWL coefficients are

$A = 2.372$ Mb
$B = 0.1061$ Mb
$R_1 = 5.6$
$R_2 = 1.8$
$w = 0.24$

The Chapman-Jouget state is given by

$P_{cj} = 0.085$ Mb
$D = 0.555$ cm/μs
$E_o = 0.057$ Mb cc/cc
$\Gamma = 2.69$
$V_{cj} = 0.724$

where D is the detonation velocity and $(\Gamma+1)/\Gamma$ defines the compression.

2.2 LUCITE

The equation of state used to describe the lucite shell was developed by Duff[8] for the KO code at Lawrence Livermore Laboratory. It fits shock velocity-particle velocity data to a straight line of the form

$$U_s = C + S\,U_p$$

where U_s is the shock velocity, U_p the particle velocity, and C and S coefficients of the fit for lucite given as

$$C = 0.251 \text{ cm}/\mu\text{s}$$
$$S = 1.545$$

The pressure is calculated from

$$P = \rho_o C^2 \mu \left[1 + \frac{2S-1}{2}\,\mu + S(S-1)\mu^2\right]$$

where

$$\mu = \frac{\rho}{\rho_o} - 1$$

and

$$\rho_o = 1.18 \text{ gm/cc}$$

Since the lucite shell was sufficiently close to the PETN to be melted, it was not necessary to specify its strength.

2.3 GROUT

Material properties tests for SRI rock matching grout (RMG 2C4) were conducted by Terra Tek.[9] Physical property and ultrasonic wave velocity measurements were made as well as mechanical property tests which included triaxial compression and uniaxial strain tests to 0.5 Kbars confining pressure. Additionally SRI has measured unconfined crush strength.[1] These measurements have been incorporated into our equation of state for grout.

Shear Failure

The material strength Y (the maximum stress difference) is chosen to be a function of $\bar{P}$ as described in Cherry, et al.[10] and is given by

$$Y = Y_o + Y_m \frac{\bar{P}}{P_m}\left(2 - \frac{\bar{P}}{P_m}\right) \qquad \bar{P} < P_m$$

$$Y = Y_o + Y_m \qquad \bar{P} \geq P_m$$

where Y_o, Y_m and P_m are constants of the fit and $\bar{P}$ is a function of the pressure P and the third deviatoric invariant J_3' (the product of the three principal deviatoric stresses). $\bar{P}$ may be written as

$$\bar{P} = P - 1/2\left(\frac{J_3'}{2}\right)^{1/3}$$

In addition, the stress difference Y is assumed to be zero at energies above the melt energy e_m (2×10^{10} ergs/gm) and to be reduced by the factor $1 - e/e_m$ for energies below e_m.

Based on both the uniaxial strain and triaxial test data, the maximum value of Y (Y_o+Y_m) was chosen as 0.33 Kbars, and P_m, the value of $\bar{P}$ at which the parabolic strength function is replaced by Y_o+Y_m, was taken to be 0.44 Kbars. The choice of individual values for Y_o and Y_m was based on the measured unconfined crush strength of approximately 0.275 Kbars. This is equivalent to Y_o of 0.21 Kbars and Y_m of 0.12 Kbars for the parabolic form.

Hooke's law is used to obtain an initial estimate of the stress deviators. Shear failure occurs if the material strength Y evaluated at $\bar{P}$ is exceeded, i.e., $\sqrt{3J_2'} > Y$, where J_2' is the second deviatoric stress invariant (one half the sum of the squares of the deviatoric stresses). If shear failure occurs, then adjustment of the stress deviators is required. We assume that each deviatoric stress component is

reduced by multiplying it by the factor f given by

$$f = \frac{Y + \frac{b}{2}\left(\frac{J_3'}{2}\right)^{1/3}}{\sqrt{3J_2'} + \frac{b}{2}\left(\frac{J_2'}{2}\right)^{1/3}}$$

where b = dY/dp is the slope of the parabolic strength function.

Tension Failure

Tension failure is assumed to occur in an element if a principal stress becomes tensile only when the element has previously failed in shear. We then apply the tension failure model proposed by Maenchen and Sack[11] and introduce an inelastic strain normal to the crack. This inelastic strain is just sufficient to zero the tensile stress (the failed element cannot support any tensile stresses) and is calculated from Hooke's law. The inelastic strain increments are accumulated during each cycle in which the principal stress is calculated to be tensile, thus giving an estimate of the crack width. Once this unadjusted principal stress becomes compressive, the crack width begins to decrease. Crack closure continues until the inelastic strain becomes zero. When this state is achieved, the element is able to support a compressive stress.

Equation of State and Pore Crushup

The Tillotson equation of state[12] together with the P-α porous rock crushup model[10] were used to describe the pressure of a rock element as a function of its energy and density. The pressure of the material without air-filled voids is given by the Tillotson equation of state as

$$P_s = \left[a + \frac{b}{\frac{e}{e_o\eta^2} + 1}\right] e\rho + A\mu + B\mu^2$$

for compressed states ($\rho > \rho_o$), and for cold expanded states ($\rho < \rho_o$ and $e < e_s$). The form

$$P_v = ae\rho + \left[\frac{be\rho}{\frac{e}{e_o\eta^2} + 1} + A\mu e^{-\beta_2(v/v_o - 1)} \right] e^{-\beta_1 (v/v_o - 1)^2}$$

is used for expanded states ($\rho < \rho_o$) when $e > e_s'$. Here $V_o = 1/\rho_o$, $\eta = \rho/\rho_o$ and $\mu = \eta - 1$. A simple approximation to the phase transition from liquid to vapor is obtained for energy states $e_s < e < e_s'$ when $\rho < \rho_o$ by calculating the pressure as

$$P = \frac{1}{e_s' - e_s} \left[(e - e_s)\ P_v + (e_s' - e)\ P_s \right]$$

e_s is the specific internal energy of the material at the vaporization temperature and e_s' includes the additional heat of vaporization required to change the material from the liquid to the vapor state. The parameters used in the fit are given in Table 1.

For a material containing air-filled voids, the pressure may be obtained from the pressure given by the Tillotson equation of state through the use of the P-α crushup model. The distension ratio α is defined as the ratio of the density of the material without voids to its density with voids included. Thus, as the grout is loaded, α decreases from its initial value $(1-\phi_o)^{-1}$, where ϕ_o is the air-filled porosity, down to 1.0 at P_c, the pressure at which all air-filled porosity is irreversibly removed. Over the early portion of the loading (the linearly elastic portion) which extends up to P_e, the elastic pressure, the porosity is assumed to be completely recoverable upon unloading. Between P_e and P_c, the plastic portion of the crush curve, the air-filled porosity is assumed to be partially recoverable on unloading.

Table 1. Summary of 2C4 Grout Material Properties Data.

Quantity	Symbol	Value	Units
Longitudinal sound speed	C	3.27	km/sec
Shear wave speed	C_s	1.82	km/sec
Density	ρ_o	2.16	gms/cc
Zero pressure bulk modulus	K_o	135.57	kbars
Shear modulus	G	71.55	kbars
Poisson's ratio	ν	0.275	
Coefficients for Tillotson Equation of State	A	150	kbars
	B	335	kbars
	β_1	5	
	β_2	5	
	a	0.5	
	b	0.633	
	e_o	6.0×10^{11}	ergs/gm
	e_{s_1}	3.5×10^{10}	ergs/gm
	e_s	1.8×10^{11}	ergs/gm
Strength Parameters	Y_o	0.21	kbars
	Y_m	0.12	kbars
	P_m	0.40	kbars
	e_m	2×10^{10}	ergs/gm
Air-filled Porosity	ϕ_o	0.007	
Elastic Pressure	P_e	0.1	kbars
Crush Pressure	P_c	1.4	kbars

Figure 3 shows the load-unload curve used for 2C4 grout and Table 1 gives the relevant material properties data. A table of values for α as a function of specific volume V may be obtained from these load-unload curves assuming that the unload curve represents the material without voids. The curves were based on a uniaxial strain test performed at Terra Tek for 2C4 grout, in which the sample was loaded only up to a pressure of 0.5 kbars and then unloaded. It appeared that the voids were not completely crushed up at 0.5 kbars. Fortunately, the same sample had been reloaded up to 4.0 kbars in another test.[13] Don Gardiner of Terra Tek has estimated the total air-filled porosity to be 0.7 percent by adding up the voids crushed up in both tests. We have estimated the crush pressure to be approximately 1.4 kbars based on these tests. The coefficients A and B for the Tillotson equation of state were chosen to be consistent with the load-unload data.

The slope of the elastic portion of the crush curve was chosen so that the zero pressure bulk and shear modulii are consistent with the measured longitudinal and shear velocities from ultrasonic tests. The choice of P_e was made to insure elastic behavior at the overburden pressure of 69 bars.

2.4 WATER

The pressurized water in the tank surrounding the grout sphere was modeled using an analytical equation of state developed by Gurtman, et al.[14] which treats the high density region near the Hugoniot up to about 300 kbars. This polynomial fit cannot however, treat expanded states, particularly if phase changes occur. These restrictions were irrelevant to the grout spheres calculation where deviations from the applied overburden were small (less than one overburden pressure). However, for the charge calibration tests, where large

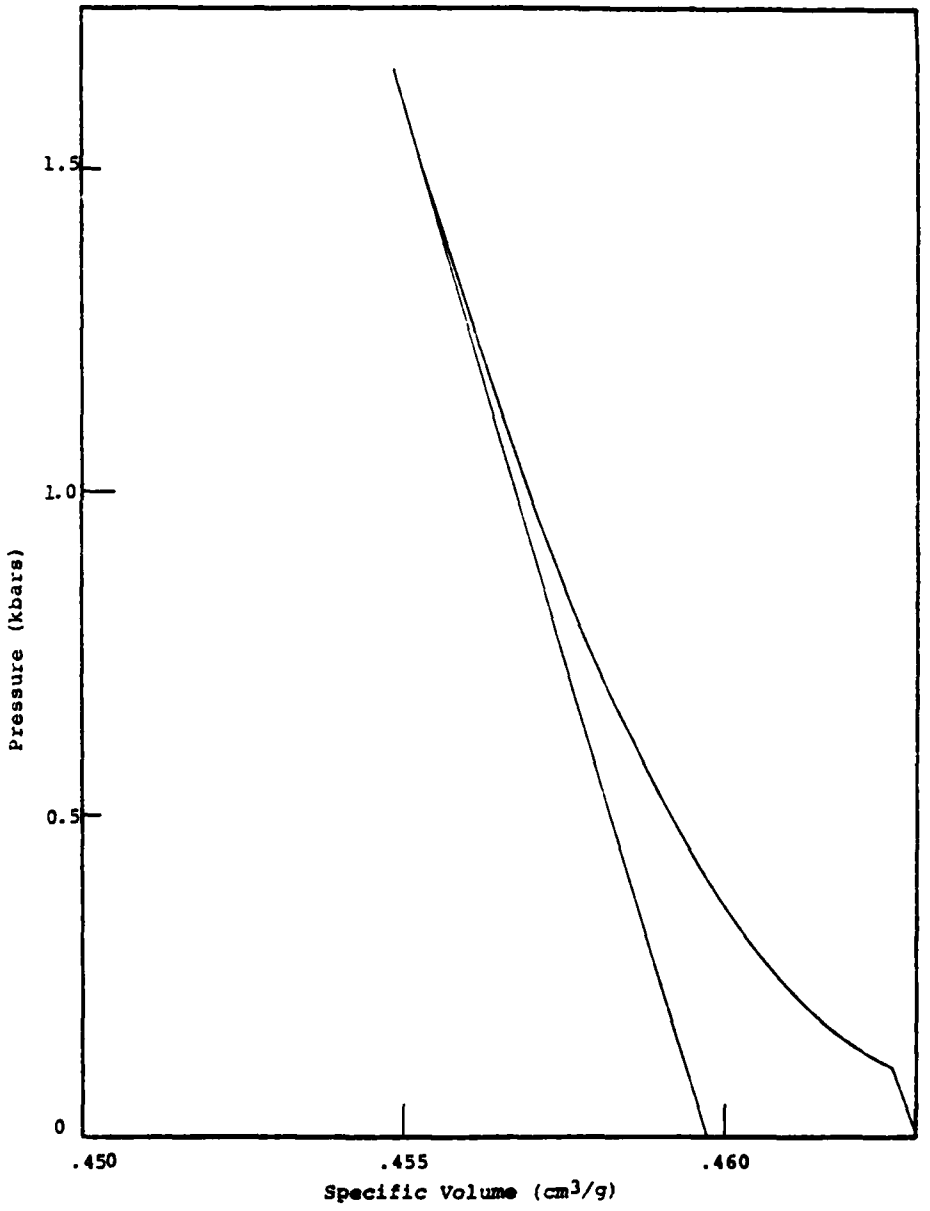

Figure 3. Load-unload curves for 2C4 grout.

shock pressures were expected and where expanded states are possible behind the shock wave, a more complete equation of state for water may be desirable.

The AQUA constitutive relations for water,[15] developed at S^3, divide the pressure-volume plane into several regions. Within the steam dome, a numerical fit to data given in the ASME steam tables is used. In the region bounded by the Hugoniot the 200 kbar release adiabat, and the liquid saturation line, an analytical fit is used. The Hugoniot is described by another analytical fit while the remainder of the P-V plane is defined by large data tables and a numerical table-lookup procedure. These tables are also extrapolated to the left of the Hugoniot.

Calculations were made for the charge calibration tests using both equations of state of water described in this section. No significant differences in the calculational results were obtained when the analytical equation of state was replaced by the AQUA package. Thus, the simpler analytical equation of state of water was used for all further calculations.

3. CHARGE CALIBRATION EXPERIMENTS

A series of experiments were made to calibrate the performance of the 3/8 gram PETN charges. These experiments consisted of detonating the charge configuration shown in Figure 4 in water in the tank shown in Figure 2. Pressure histories at various locations were measured by means of a piezoresistive ytterbium gauge and a piezoelectric quartz pressure transducer. The ytterbium gauge was allowed to follow the motion of the water so that a direct measurement of shock wave pressure was obtained. However, the quartz gauge was rigidly mounted in the bottom of the tank and measured reflected pressure. The integrated signal is therefore reflected impulse.

Table 2 shows the results of 12 charge calibration experiments for the nominally 3/8 gm PETN charge (the actual weight of PETN is given for each shot). Peak incident pressure and impulse are given for the quartz gauge as one-half the corresponding values for the reflected wave. Also presented in Table 2 are peak incident pressures measured by the ytterbium gauge at various locations. Note that the quantities measured by the two gauges do not have a consistent pattern from shot to shot. For example, consider shots 20, 21, and 22. Based on charge weight, one would expect the largest peak pressures and impulses to occur for shot 20. However, the maximum impulse at the quartz gauge is approximately 16 percent less than for shot 22. (The ytterbium gauge gave close agreement between peak pressures for these 2 shots.) Similarly, a comparison between shots 20 and 21 shows slightly larger impulse at the quartz gauge for shot 21, but 28 percent smaller peak pressure at the ytterbium gauge. The variability in these results seems to be at least partly due to ringing in the quartz gauge. Fortunately most of the integrated impulses are in better agreement (shots 12 through 17). A characteristic of the data is that all records integrated electronically give almost the same impulse.

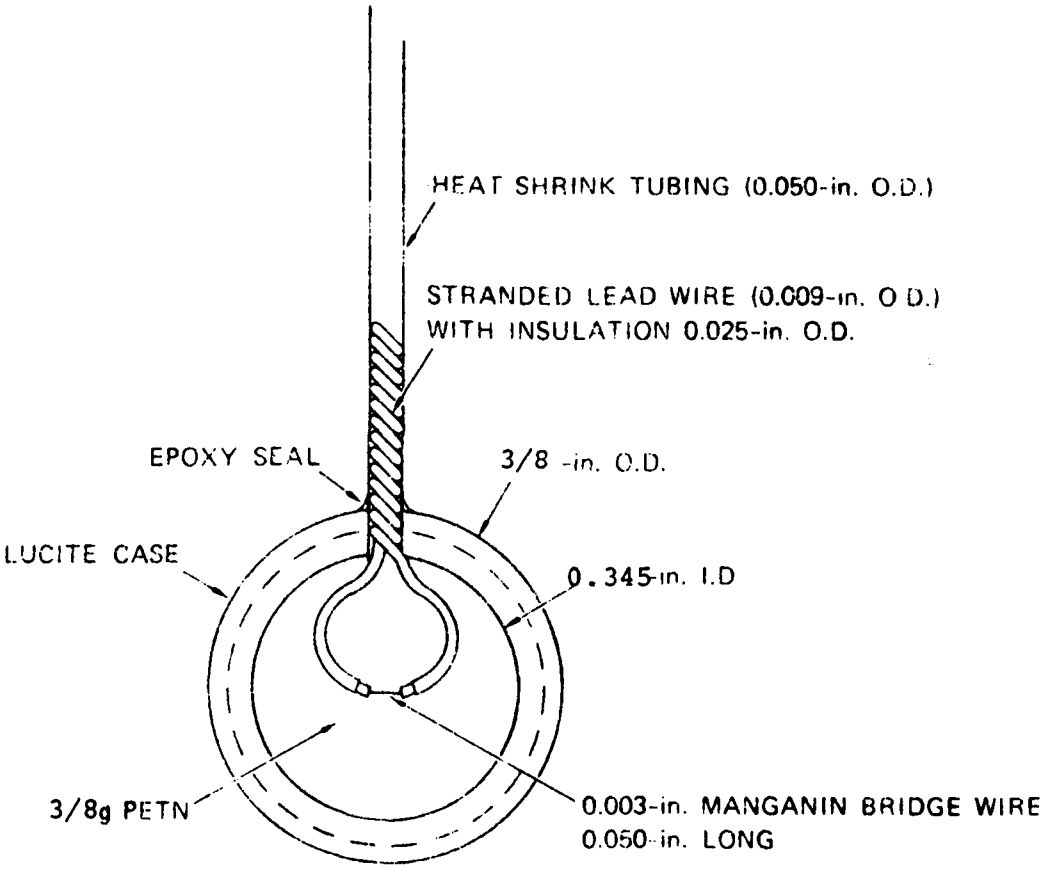

Figure 4. Explosive charge details (3/8 gram).

Table 2. Summary of Results for 3/8-Gram Charges

Shot No.	Weight of PETN (g)	QUARTZ GAUGE			YTTERBIUM GAUGE	
		Distance from center of charge to gauge (in.)	Peak incident pressure (psi)	Maximum incident impulse (psi-μsec)	Distance from lucite surface to gauge (in.)	Peak incident pressure (psi)
10	0.3630	6-5/8	3500	-	7/16	-
11	0.3644		4750	-	7/16	-
12	0.3634		3125	50,000(E)	7/16	54,100
13	0.3566		4125	50,500(E)	7/16	-
14	0.3586		4000	50,500(E)	7/16	56,600
15	0.3672		4125	50,500(E)	7/16	55,900
16	0.3587		2875	50,500(E)	7/16	55,800
17	0.3619		3375	51,000(E)	7/16	50,750
20	0.3701		3250	53,500(M)	1/4	130,500
21	0.3679		4500	55,000(M)	1/4	102,600
22	0.3674		4875	62,000(M)	1/4	137,800
23	0.3794		4625	59,500(M)	1/8	144,700

(E) = Electronic integration

(M) = Mechanical integration

Two calculations have been performed using SKIPPER to simulate these experiments. One used the AQUA equation of state for water and the other a simpler analytical fit. Use of the different water equations of state produced only negligible differences in the calculated results. The constitutive modeling used for the PETN and lucite have been discussed in Section 2 of this report. The explosive charge configuration has been simplified to conform to the spherical geometry of the calculation. A 3/8 gm spherical charge was used in the calculation and the bridge wire was eliminated. This gave a radius of PETN slightly larger than reported by SRI (0.447 cm rather than 0.438 cm). Since the outer radius of the lucite (0.476 cm) was the same as in Figure 4, we have slightly more PETN (see Table 2) and less lucite for our calculation.

A comparison of the calculated and measured peak pressures vs. range are shown in Figure 5. The dashed curve indicates the relationship predicted for explosive charges in water by Langefors and Kehlstrom.[16] This relationship was compiled from many sources and includes measurements over ranges of pressures from 10 GPa (100 kbars) down to 10 MPa (100 bars). Our calculation is in excellent agreement with these predictions. At the three in-close stations (range less than 2 cm), the calculated peak pressures agree well with the ytterbium gauge measurements. The slightly low measurement at the first station is probably not significant when compared with the scatter at the second station.

The reflected peak pressures measured at the quartz gauge are considerably higher than those determined by the calculation (approximately a factor of two on the average). A portion of our calculation was redone with finer zoning. This only resulted in a 10 percent increase in peak reflected pressure and did not alter the total impulse. Figure 6 compares the pressure history calculated at the quartz gauge with the gauge record for shot 15 of Table 2. The gauge

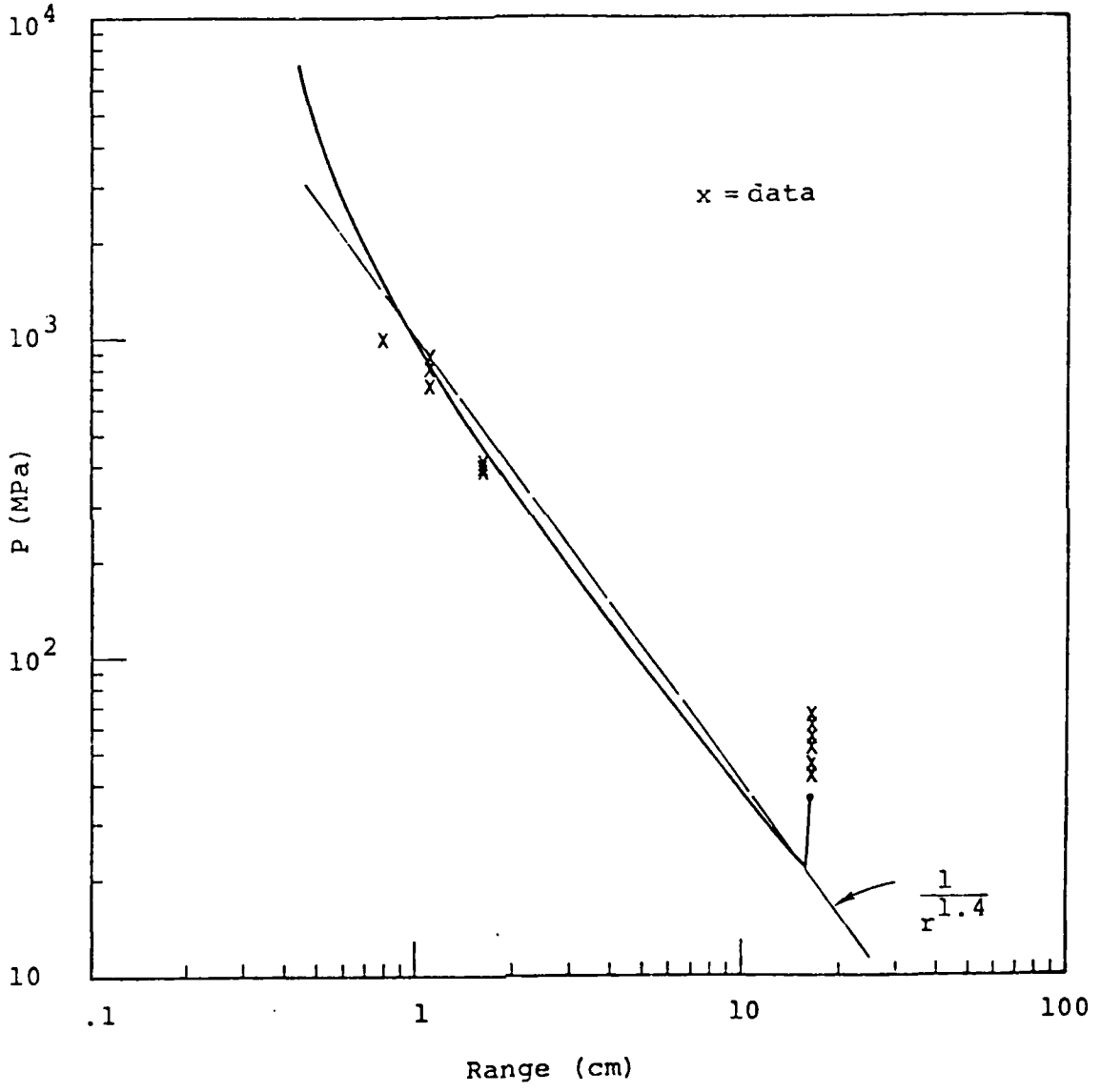

Figure 5. Calculated peak pressure vs. range compared to ytterbium and quartz experimental data points. The dashed line gives the relation expected for an explosive charge in water.

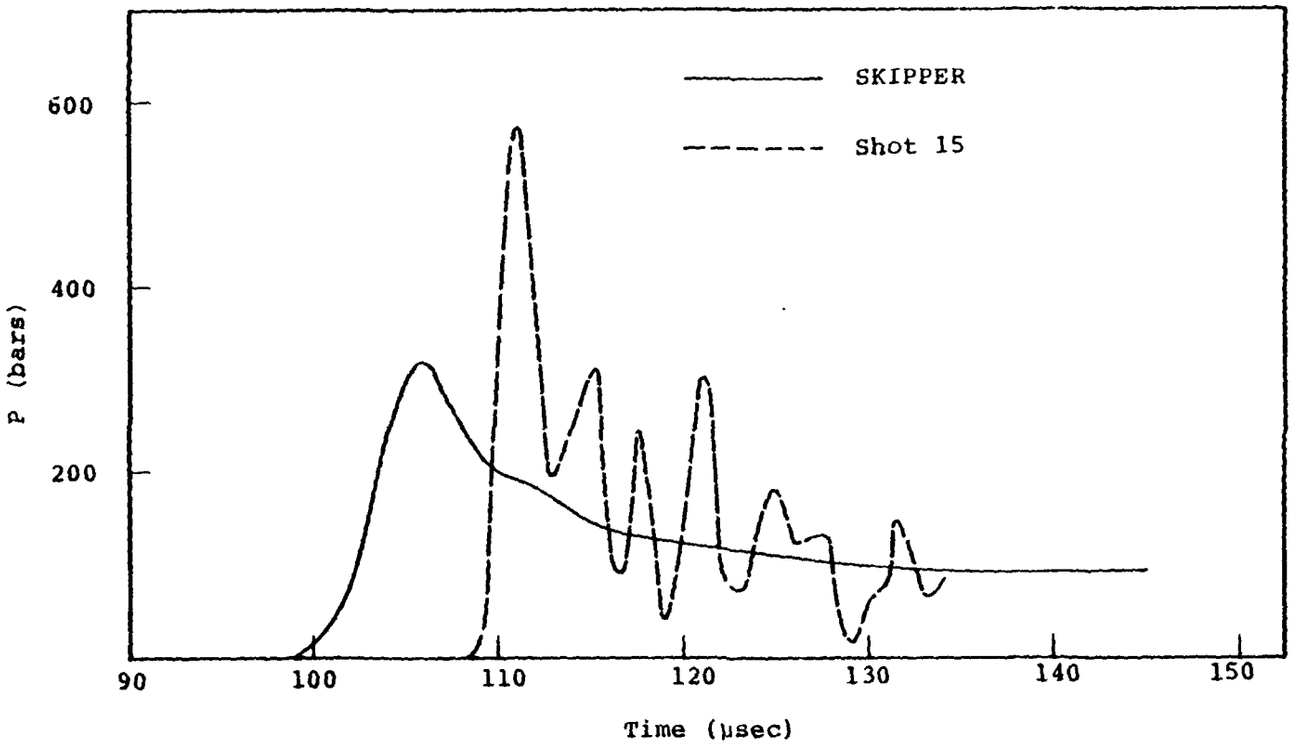

Figure 6. Comparison between SKIPPER calculation of the pressure pulse at the quartz gauge and Shot 15 data.

record indicates severe nonphysical ringing. If the peaks and valleys are averaged and a smooth curve drawn through the average, the true peak pressure is probably approximately 30 MPa, which is in excellent agreement with the calculations. The SKIPPER calculation shows an arrival time approximately 9 microseconds earlier than indicated by the data. This may possibly be due to a small error in estimating the EDU delay. If the calculated pulse were displaced 9 microseconds in time, excellent agreement would be obtained between the calculated results and the smooth curve drawn through the ringing quartz data.

A comparison of the calculated and measured impulse at the quartz gauge for shot 15 (the integral of the waveform of Figure 5) is shown in Figure 7. Except for the difference in arrivals, the two curves are in remarkable agreement, particularly when one considers the shape of the measured pressure history, and the fact that the quartz gauge is in the bottom of a cylindrical tank, whereas the calculation assumes spherical geometry. At times greater than about 150 microseconds the possible influence of reverberations off the sides of the cylindrical tank on the measured signal should cause our calculated impulse to differ from the data. The calculation was therefore terminated.

The results shown in this section have shown that we can accurately calculate the detonation of the PETN and the wave propagation through the lucite and water using the SKIPPER code. It also seems clear that SRI has demonstrated reproducibility for its 3/8 charges at least to within 20 percent for the measured impulse. The measured impulse at the quartz gauge should be a useful measurement for the grout spheres experiments to be conducted in the future in order to calibrate whether the variability in hydrofracture records is due to variations in the PETN detonation and dynamic propagation through the grout.

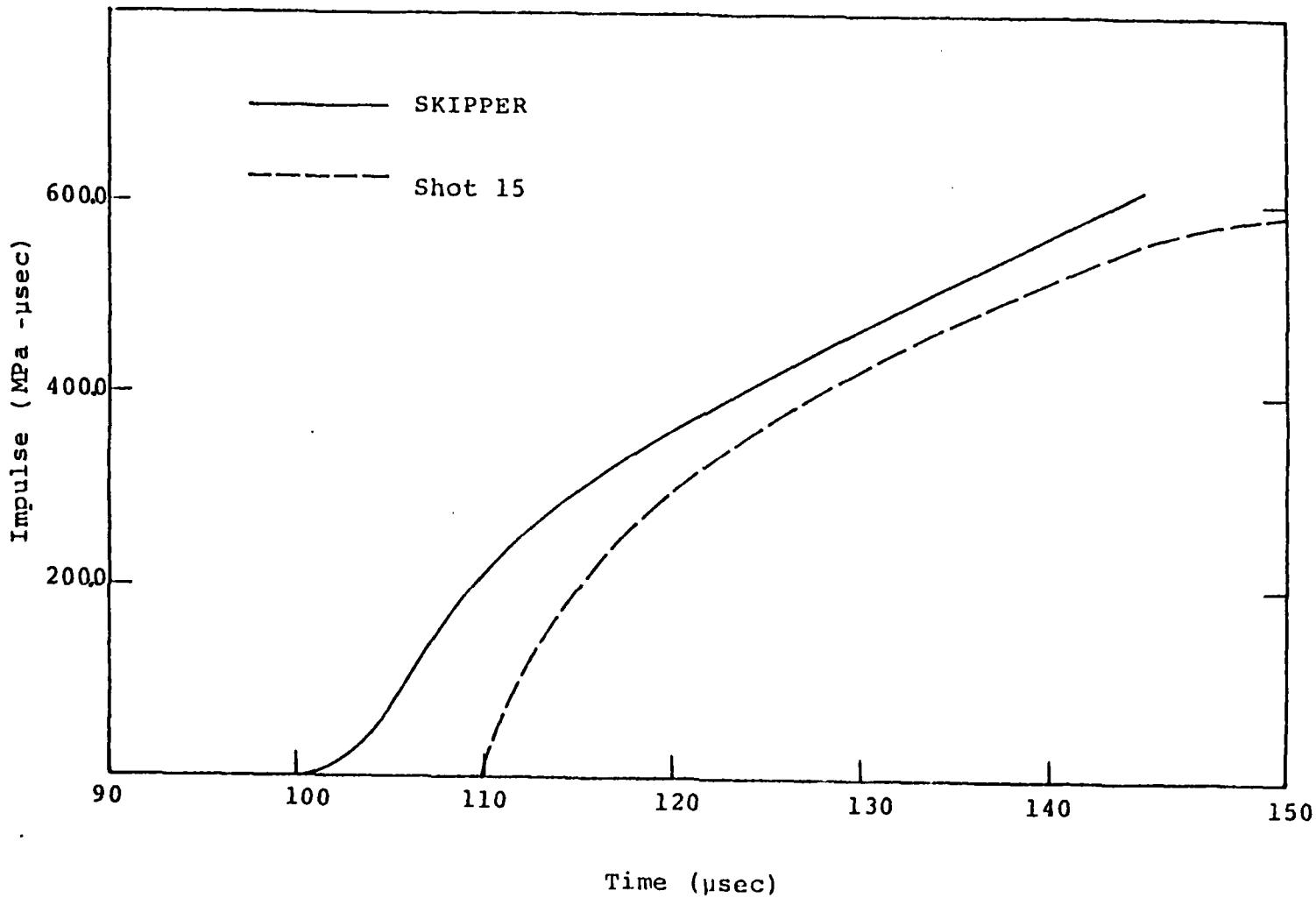

Figure 7. Calculated impulse compared to integrated quartz pressure history.

4. COMPUTATION OF THE RESIDUAL STRESS FIELD IN THE GROUT

Calculations were performed of the detonation of the 3/8 gm PETN charge placed in a 12 inch diameter sphere of 2C4 grout. Constitutive models and material properties used in the calculations have been presented in Section 2, and the configuration of the charge (PETN plus lucite) has been discussed in Section 3. The sphere was surrounded by water at an overburden pressure of 6.8 MPa, and a rigid boundary simulating the quartz gauge in the bottom of the tank was placed 17.8 cm from the charge center.

The calculations showed extensive tensile cracking after passage of the shock wave both in the first 0.857 cm (0.5 cm thick after cavity expansion) of grout adjacent to the lucite and in an interior region extending radially from approximately 5.1 to 7.5 cm. These cracks were all in the radial direction (the hoop stress became tensile). Those cracks near the explosively formed cavity closed during cavity rebound. However, the permeability of this region almost certainly has been increased due to the tensile cracking. Examination of the exploded spheres after hydrofracture shows a heavily stained rubble region extending approximately 1/4 inch (0.6 cm) which indicates complete penetration by the hydrofracture fluid that could be due to increased permeability.

The tensile cracks in the interior region of the grout do not close completely. Figure 8 shows the calculated residual stress field in the grout. The radial stress σ_r is continuous. However, the plot of hoop stress σ_t shows a small bump in the previously cracked region at a radius of approximately 6 cm, just before the remaining open portion of the crack (where σ_t is zero). Both stress components are equal to the applied overburden in the water at 15.2 cm.

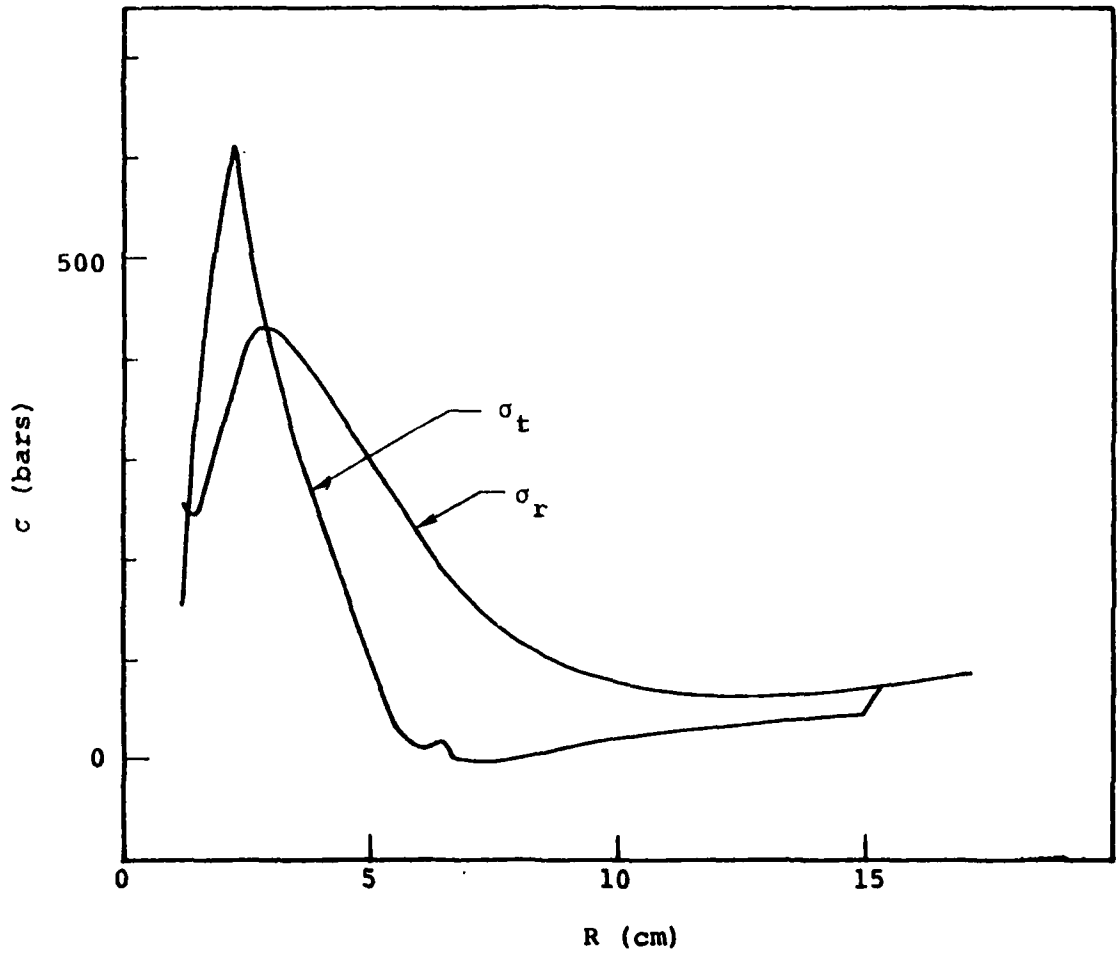

Figure 8. Residual stress field for 3/8 gm charge in 2C4 grout.

Due to the presence of a rigid boundary in the calculations at the location of the quartz gauge, almost constant oscillations with variations of 200 bars in peak residual stress were calculated as a wave was reflected off the boundary propagated inward and was reflected again at the cavity. As the oscillation passed, the remaining tensile cracks opened and closed. These oscillations tended to continue throughout the grid to late times. To obtain our final residual stress field, the coefficient of linear artificial viscosity was increased a factor of 10, thus damping out this oscillation.

The cavity radius corresponding to the final residual stress state was calculated as 1.21 cm and the cavity gas pressure as 251 bars. It should be pointed out that this calculated cavity pressure is considerably larger than the average fracture initiation pressure for all 3/8 gm charge tests which is 185 bars (2687 psi). We believe that a creep or stress relaxation process takes place in the time between the formation of the residual stress field and the hydrofracture of the grout spheres. This process reduces the magnitude of the compressive residual stress field so that the hydrofracture can occur at lower pressures. There is some experimental evidence to support this hypothesis. Grout spheres that are left standing many hours before hydrofracturing give lower fracture initiation pressures. In addition, cavities which have not been vented (venting should accentuate the creep process) give significantly larger fracture initiation pressures.

The measured cavity radii for the 3/8 gm charge tests are approximately 0.95 cm (3/4 inch) which is 27 percent lower than the calculated value. However, the radius measurements take place after the sphere is cracked open, i.e., after creep, venting, and hydrofracture have occurred. There is little reason to believe that these processes have not altered the cavity radius from its value immediately after charge detonation.

One purpose of the quartz gauge is to test and validate predictions in order to gain some understanding of the phenomenology. Figure 9 shows the calculated overpressure vs. time at the quartz gauge and Figure 10 the calculated total impulse, obtained by integrating the data of Figure 9. Recent SRI data[17] for tests 138 and 139 showed peak incident overpressures of 530 (3.654) and 550 psi (3.792 MPa). Maximum incident impulses were 6200 (42.7) and 6500 psi·μsec (44.8 MPa·μsec). The reflected values for comparison with our calculations are twice the incident giving an average measured peak overpressure of 74.6 bars (7.46 MPa) and an average maximum impulse of 873 bars-μsec (87.3 MPa-μsec). Our calculated maximum values are 45.5 bars overpressure and 735 bars-μsec maximum impulse.

As discussed in Section 3, the pressure measurement (see Figure 6) shows a great deal of nonphysical ringing. Extrapolating from the signal shown in Section 3 (we do not have the pressure histories from shots 138 and 139), the reported peak overpressure could be high by almost a factor of 2. Thus, a comparison between measured and calculated peak overpressures is probably not meaningful in the absence of a full pressure history. However, the integrated signal (the impulse) has been shown in Section 3 to give good agreement with calculations even for a ringing pressure history. Therefore, a comparison between measured and calculated maximum impulse is meaningful. Our calculation gave a 15 percent lower impulse than the average of shots 138 and 139, well within the 20 percent variability of the charge calibration test results given in Table 2 of Section 3. Since the constitutive models and materials properties data are not an accurate model of the grout to better than 10 percent, the agreement between the measured and calculated impulses appears excellent.

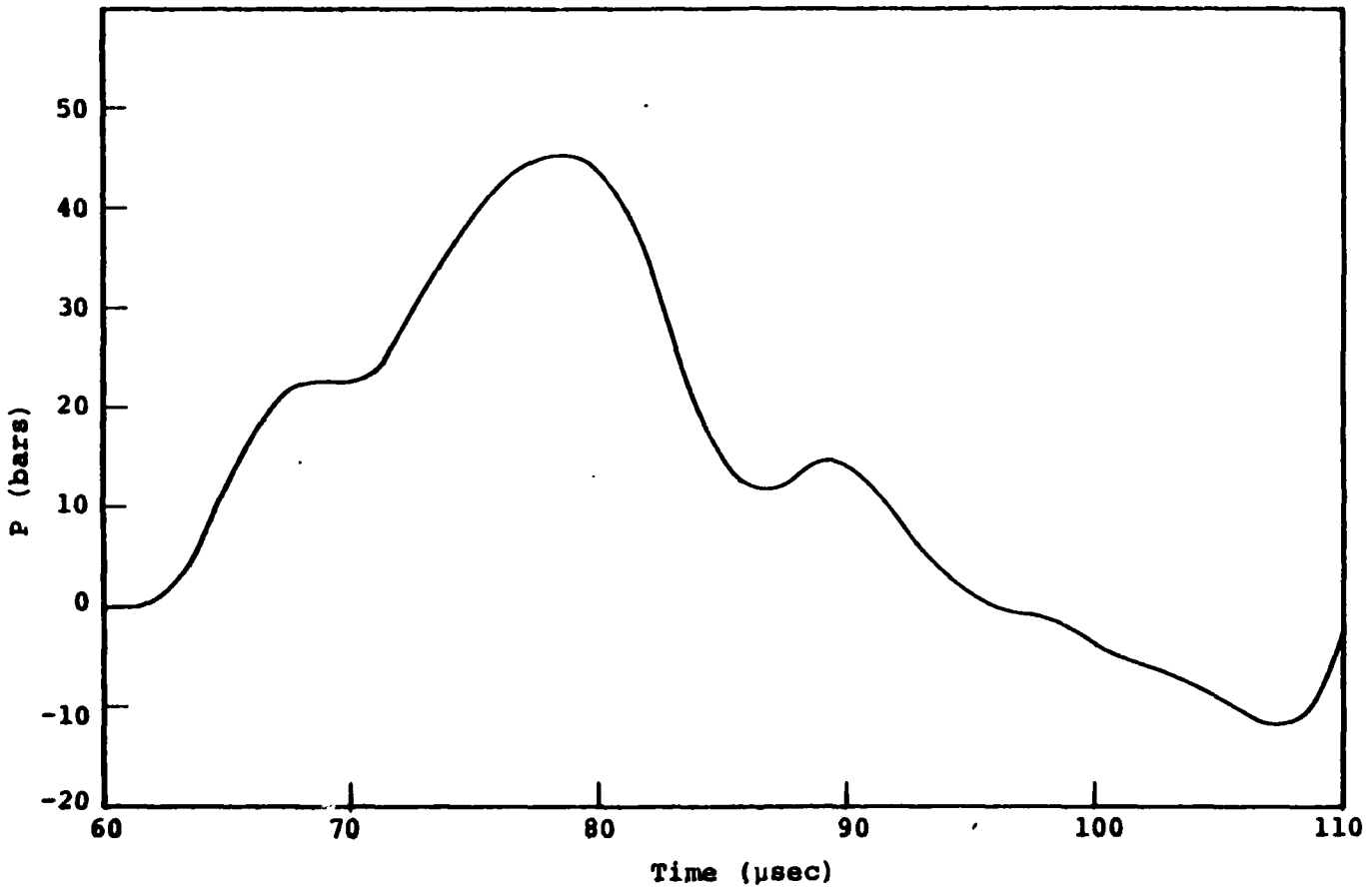

Figure 9. Overpressure at the quartz gauge (7") for 3/8 gm grout sphere calculation (overburden = 69 bars).

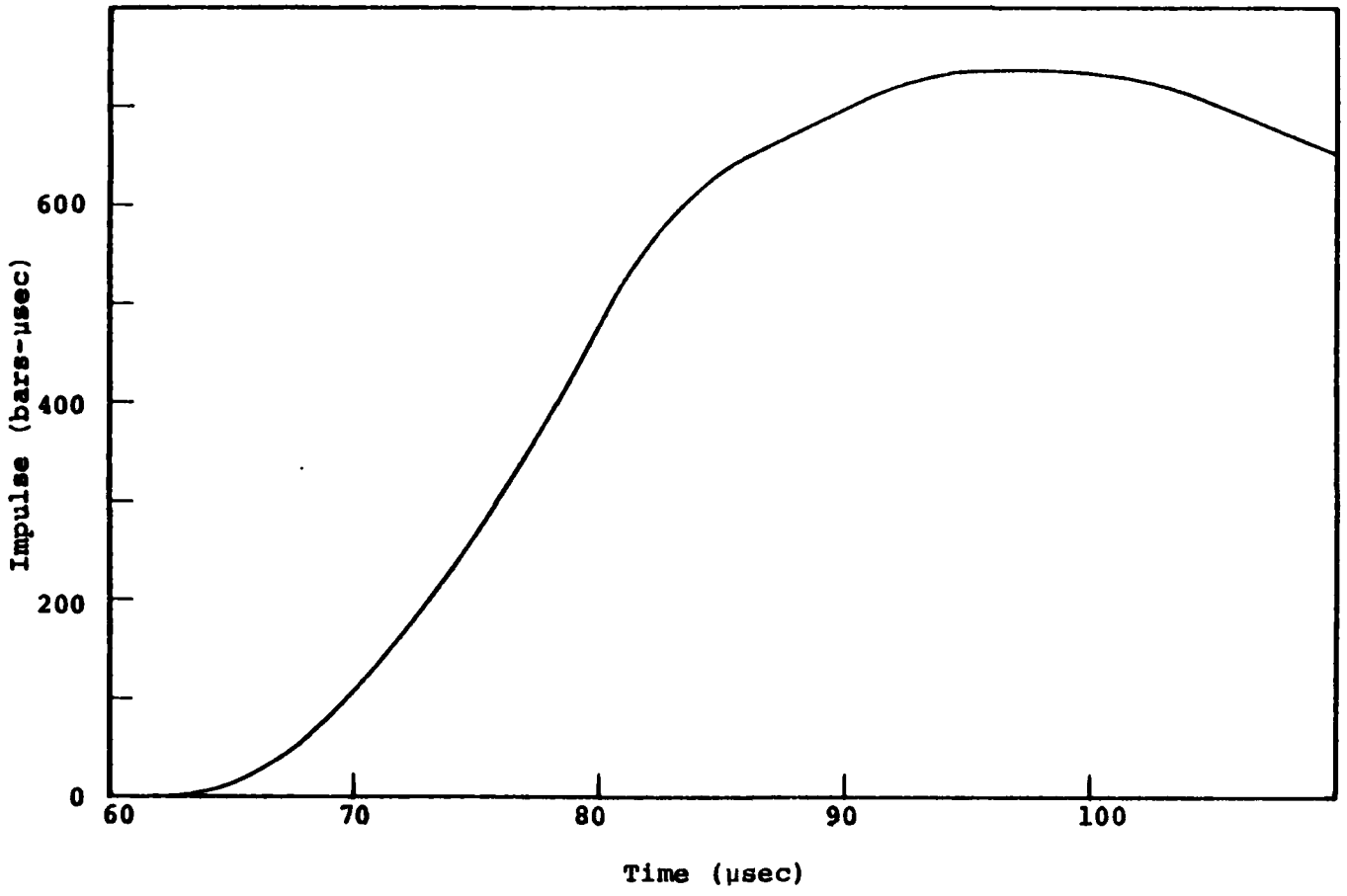

Figure 10. Impulse at the quartz gauge (7") for 3/8 gm grout sphere calculation.

5. A NUMERICAL MODEL OF THE VENTING AND SPHERICALLY SYMMETRIC FRACTURE INITIATION

A majority of the SRI exploded sphere hydrofracture tests show one major crack extending out of the cavity region (as indicated by the dye in the hydrofracture fluid). Therefore, a numerical model of these tests should be two-dimensional (see Klein[5]). However, some of the SRI tests (shots 68 and 77) are examples) show a network of cracks extending radially from the cavity. These tests also require considerably greater pressures in order to hydrofracture the spheres. In order to explain these tests, a simplified one-dimensional spherically symmetric model of quasi-static crack propagation through a residual stress field was developed by Narasimhan.[4] The results obtained from the model provide an upper bound for the hydrofracture experiments and are useful in describing some of the qualitative features of the experiments, i.e., the effects of impermeable membranes or jackets on the inside or outside of the sphere.

Several of the assumptions in the simplified model[4] are in conflict with the residual stress fields calculated here using the SKIPPER code (see Figure 8). In the simplified model, the residual stress field for most cases studied is represented by an analytical expression which results in a zero tangential stress at the outer radius of the sphere and therefore immediate unstable crack propagation for the unjacketed case. A few cases assumed a hoop stress equal to one-half the overburden pressure. The SKIPPER calculations show a significant hoop stress near the outside of the sphere. Also, the simplified model assumed the grout sphere to be uncracked initially before hydrofracture, but the calculations show unclosed cracks. Finally, excursions from the residual stress state were assumed to be linearly elastic.

Here we attempt to use the SKIPPER code to simulate the venting of the high pressure explosive gases from the cavity and the subsequent spherically symmetric hydrofracture of the grout sphere from this cavity. In this way, we can use the actual calculated residual stress fields including the tensile cracks and permit the grout to yield plastically during hydrofracture. In this section, results are presented which indicate that this numerical procedure can be used successfully to model hydrofracture. We should emphasize that these results are only preliminary. Further numerical tests are presently being made to determine the sensitivity of the solutions to zoning and to unloading and reloading rates.

Figure 11 shows the hoop stress in the first grid zone of the grout sphere adjacent to the cavity as the pressure in the cavity is unloaded (simulating venting) and reloaded (simulating the onset of hydrofracture). Unload was accomplished by reducing the cavity energy linearly in increments of time, thus reducing the cavity pressure through the JWL equation of state for the PETN detonation products. Two unloads were made down to a pressure of 1.0 bar, one in a time of 30 microseconds and the second in 70 microseconds. Point A in Figure 11 gives the initial stress state in zone 1 of the SKIPPER grid after the dynamic calculation has been completed (the cavity pressure is approximately the same as the radial stress in zone 1). As the cavity pressure is decreased, σ_t tends to increase (hoop stress becomes more compressive). Point B indicates the onset of yielding in zone 1 for the 70 microsecond unload. This calculation was continued for approximately 60 microseconds after the unload pressure of 1 bar was reached. At this time, the hoop stress had relaxed down to point C (σ_t = 222 bars). Although the faster unload calculation (30 microseconds) showed a different unload path, the final stress state was in fairly good agreement (σ_t = 230 bars).

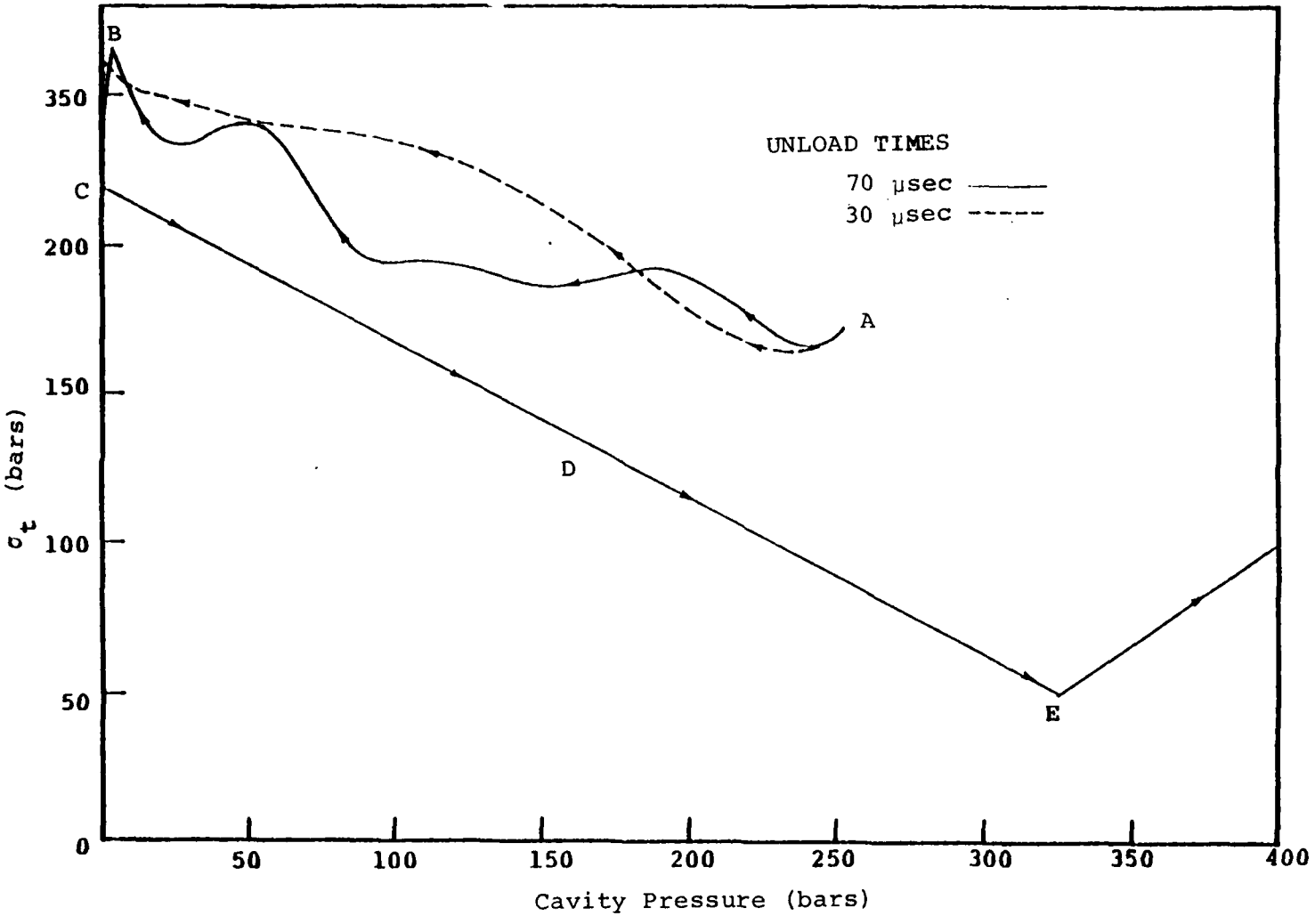

Figure 11. Hoop stress vs. cavity pressure in first grid zone as the cavity is vented and hydrofractures. Point A is stress state before venting; Point B indicates yielding; Point C is starting point for reload; Point D is when $\sigma_t < P$; Point E indicates yielding.

In these preliminary calculations, no attempt was made to unload in a time comparable to the actual venting time (tenths of seconds to seconds). Thus, the unload was not quasistatic (the transit time of a wave from the cavity to the outside of the sphere and back is approximately 100 microseconds and the time to the residual stress peaks and back approximately 60 microseconds). Negligible changes in cavity radius and peak residual stress resulted from the unload. We should emphasize that time dependent creep phenomena which might be expected to reduce the stress fields were not included in the model. It remains to be seen what the effect of a slower unload would be. This can be accomplished by a rezone of the grid near the cavity which would greatly increase the time step (the first zone in the preliminary calculations was approximately 0.005 cm thick).

Starting from the stress state given by point C of Figure 11, the hydrofracture of the grout sphere was simulated by a time dependent pressure boundary condition on the surface of the vented cavity. Loading was at the rate of 72 bars of cavity pressure/msec, i.e., much more rapidly than in the experiment. There was an initial oscillation in σ_t in zone 1 up to pressures of 40 bars but in general σ_t tended to decrease at a rate one-half as great as the loading rate. At point D along the loading path σ_t became less than P in zone 1 for the first time. At this point, cavity pressure was 138 bars (2030 psi), slightly lower than measured fracture initiation pressures. The actual fracture initiation pressure depends on inhomogeneities in the grout at the cavity boundary which will initiate cracking once a stress condition is reached which will propagate a crack. It has been speculated that if the hydrofracture fluid (at cavity pressure) can find a path into the grout, the stress state given by point D in Figure 11 can represent the minimum value of the fracture initiation pressure. Our calculational model attached no

special significance to this stress state for the present calculations. However, the cracked region adjacent to the cavity described earlier for the dynamic calculations does indicate a path into the grout.

The cavity loading was continued to test whether the hoop stress σ_t became tensile (the cracking criteria used by Narasimhan[4]). Figure 11 shows that σ_t continued to decrease until stress state E was reached, but that from then on σ_t increased as loading continued. Point E indicates the onset of yielding in zone 1. At this point, the stress path changes from a path characterized by constant mean stress in zone 1 and increasing deviatoric stress in the radial direction (the reason for the slope of one-half in Figure 11) to a path characterized by increasing mean stress as well. As loading continues, more and more zones begin to yield and σ_t continues to increase. The cracking criteria of Narasimhan for elastic loading did not appear to be reachable, so the calculation was terminated.

If future sensitivity tests show that the preliminary results given here are valid, a different cracking criterion must be developed, possibly based on some critical difference between σ_r and σ_t or on a strain criterion. Once a cell is cracked, cavity pressure will be assumed in that cell, and the calculation continued. We hope to be able to develop this calculational tool to investigate the grout spheres problem further. Some parametric modification of the residual stress fields before unloading to simulate creep seems also worthy of further study.

We have also looked at the possibility of investigating the quasistatic features of the grout spheres experiments with a one-dimensional finite element code. At present, it appears more cost effective to use the SKIPPER code which includes the desired constitutive models rather than to incorporate these models into a finite element code.

6. SUMMARY AND CONCLUSIONS

In this report, we have discussed the present status of one aspect of our numerical simulation of the SRI grout spheres containment experiments. We have demonstrated our ability to correctly calculate containment-related phenomena, in particular, a high explosive detonation and the subsequent propagation of nonlinear waves through media such as grout, lucite, and water. Also, we have introduced a simple model which may be useful in explaining some features of the experiment. This model uses the SKIPPER code to examine both the effects of venting on the calculated residual stress fields, and, hopefully, also to study the onset and propagation of radial fractures from the cavity induced by the hydrofracture fluid.

In this section, we summarize our results and conclusions relative to the various phases of the grout spheres experiments.

6.1 CHARGE CALIBRATION TESTS

The SRI charge calibration tests involved exploding the 3/8 gm PETN charge surrounded by a thin lucite shell in a water tank and measuring peak stresses using a nearby ytterbium gauge. Stress histories were also measured using a quartz gauge imbedded in the wall of the tank. Calculated peak stresses vs. range are in excellent agreement both with the literature[16] and with the ytterbium data. The calculation lies well within the scatter of the ytterbium data. Calculated peak reflected pressure was a factor of 2 lower than the reported data probably due to severe ringing in the quartz gauge. If the ringing is averaged out, the data then is in excellent agreement with the calculated history (except for a 9 microsecond difference in signal arrival which is possibly due to an inaccurate estimate of EDU delay). The integrated signal (the impulse) is in excellent agreement with the calculated impulse in spite of the ringing gauge.

The results for a series of 12 charge calibration tests indicate that the measured impulse is reproducible to within 20 percent. Thus, it will be very useful to implace a quartz gauge for every future grout spheres tests in order to check out the charge detonation.

6.2 RESIDUAL STRESSES IN A GROUT SPHERE

Unfortunately, very little data exists with which to compare our calculated residual stress fields. Our calculated impulse agrees with the quartz gauge data to 15 percent, within the 20 percent variability of the charge calibration test results. As before, our calculated peak pressures are much lower than the reported data possibly due to ringing in the quartz gauge. We are also able to calculate a 0.5 cm thick region of tensile cracks adjacent to the explosively generated cavity which close after cavity rebound. These cracks result in an increased permeability which is seen as a heavily stained region around the cavity after the experiment when the spheres are split open.

The calculated cavity pressure before venting is approximately 30 percent greater than the average fracture initiation pressure from the latest SRI exploded sphere tests. We believe that a creep or stress relaxation process takes place in the time between the formation of the residual stress field and the hydrofracture of the grout spheres that reduces the magnitude of these stresses so that hydrofracture can occur at lower pressures. Experiments show that grout spheres left in the tank for hours after venting hydrofracture at lower pressures than those hydrofractured immediately. Also, tests in which the cavity gases are not vented, and in which reload takes place relatively quickly require higher fracture initiation pressure. Finally, preliminary results using the simple calculational model described in Section 5 indicate that the venting itself does not significantly reduce

the residual stress field. These all indicate the presence of a time-related stress relaxation process. For this reason, we strongly recommend that all future explosive sphere tests use unvented cavities and that they begin as soon as possible after detonation. We also suggest that creep measurements of some sort be made in order to guide development of a creep model.

REFERENCES

1. Cizek, J. C. and A. L. Florence, "Laboratory Investigation of Containment in Underground Nuclear Tests," Stanford Research Institute Draft Final Report, SRI PYU-5958; submitted to DNA January 1978.

2. Florence, A. L., "Laboratory Investigation of Stemming and Containment in Underground Nuclear Tests," SRI Final Report, DNA 4149F, October 1976.

3. Cizek, J. C. and A. L. Florence, "Laboratory Investigations of Stemming and Containment in Underground Nuclear Tests," SRI Bimonthly Progress Report No. 8, May 1978.

4. Narasimhan, K., "Hydrofracture in a Thick Spherical Shell with Residual Stress," SSS Topical Report SSS-R-78-3612, April 1978.

5. Klein, L., "A Finite Element-Finite Difference Model for Crack Propagation in Geological Media Under Internal Pressure," SSS Topical Report SSS-R-78-3613, April 1978.

6. Lee, E., M. Finger and W. Collins, "JWL Equation of State Coefficients for High Explosives," Lawrence Livermore Laboratory Report UCID-16189, January 1973.

7. Finger, M., Private communication, June 1976.

8. Duff, R., Private communication, July 1977.

9. Gardiner, D. S., Terra Tek, Inc., Letter to A. Florence, SRI, July 8, 1977.

10. Cherry, J. T., N. Rimer and W. O. Wray, "Seismic Coupling from a Nuclear Explosion: The Dependence of the Reduced Displacement Potential on the Nonlinear Behavior of the Near Source Rock Environment," SSS Technical Report SSS-R-76-2742, September 1975.

11. Maenchen, G. and S. Sack, "The Tensor Code" in Methods in Computational Physics, Vol. 3, Academic Press, New York, 1964.

12. Tillotson, J. H., "Metallic Equations of State for Hypervelocity Impact," General Atomic Report GA-3216, July 1962.

13. Gardiner, D. S., Terra Tek, Inc., private communication.

14. Gurtman, G. A., J. W. Kirsch and C. R. Hastings, "Analytical Equation of State of Water Compressed to 300 Kilobars," J. Appl. Physics 42, p. 851, 1971.

15. Pritchett, J. W. and M. H. Rice, "User's Guide to the AQUA Subprogram Sustem -- A Comprehensive Constitutive Package for Water," SSS Internal Report SSS-IR-75-2544, January 1975 (S^3 proprietary data).

16. Langefors, U. and B. Kihlstrom, "The Modern Technique of Rock Blasting," Wiley and Sons, New York, pp. 348, 1967.

17. Cizek, J. C. and A. L. Florence, "Laboratory Investigation of Stemming and Containment in Underground Tests," SRI Bimonthly Progress Report No. 9, July 1978.

DISTRIBUTION LIST

DEPARTMENT OF DEFENSE

Defense Nuclear Agency
ATTN: SPTD, T. Kennedy
4 cy ATTN: TITL

Defense Technical Information Center
12 cy ATTN: DD

Field Command
Defense Nuclear Agency
ATTN: FCTMD, W. Summa

Field Command Test Directorate
Defense Nuclear Agency
ATTN: FCTC, J. LaComb

Field Command
Defense Nuclear Agency
ATTN: FCTK, C. Keller

DEPARTMENT OF ENERGY

Department of Energy
Nevada Operations Office
ATTN: R. Newman

DEPARTMENT OF ENERGY CONTRACTORS

Los Alamos Scientific Laboratory
ATTN: R. Brownlee
ATTN: E. Jones
ATTN: F. App
ATTN: A. Davis
ATTN: L. Germain

DEPARTMENT OF ENERGY CONTRACTORS (Continued)

Lawrence Livermore Laboratory
ATTN: D. Oakley
ATTN: B. Hudson
ATTN: B. Terhune
ATTN: J. Shearer

Sandia Laboratories
ATTN: C. Mehl
ATTN: C. Smith

OTHER GOVERNMENT AGENCY

Department of the Interior
U.S. Geological Survey
ATTN: R. Carroll

DEPARTMENT OF DEFENSE CONTRACTORS

Pacifica Technology
ATTN: G. Kent

General Electric Company—TEMPO
ATTN: DASIAC

Physics International Co.
ATTN: E. Moore

SRI International
ATTN: A. Florence

Systems, Science & Software, Inc.
ATTN: R. Duff

Terra Tek, Inc.
ATTN: S. Green